JBC RESEARCH ARTICLE

# Molecular basis for substrate recognition by the bacterial nucleoside transporter NupG

Received for publication, November 28, 2020, and in revised form, February 22, 2021 Published, Papers in Press, February 26, 2021,
https://doi.org/10.1016/j.jbc.2021.100479

**Chen Wang[1,‡], Qingjie Xiao[1,‡], Huaichuan Duan[2,‡], Jinhong Li[1], Jiying Zhang[1], Qisheng Wang[3], Li Guo[1], Jianping Hu[2,*], Bo Sun[3,*], and Dong Deng[1,*]**

*From the [1]Key Laboratory of Birth Defects and Related Disease of Women and Children of MOE, State Key Laboratory of Biotherapy, Department of Obstetrics, West China Second Hospital, Sichuan University, Chengdu, China; [2]School of Pharmacy, Sichuan Industrial Institute of Antibiotics, Chengdu University, Chengdu, China; [3]Shanghai Synchrotron Radiation Facility, Shanghai Advanced Research Institute, Chinese Academy of Sciences, Shanghai, China*

Edited by Mike Shipston

**Nucleoside homeostasis, which is mediated by transporters and channels, is essential for all life on Earth. In *Escherichia coli*, NupG mediates the transport of nucleosides and was deemed to be the prototype of the nucleoside proton symporter (NHS) family and the major facilitator superfamily. To date, the substrate recognition and transport mechanisms of NHS transporters are still elusive. Here, we report two crystal structures of NupG (WT and D323A NupG) resolved at 3.0 Å. Both structures reveal an identical inward-open conformation. Together with molecular docking and molecular dynamics simulations and *in vitro* uridine-binding assays, we found that the uridine binding site, which locates in the central cavity between N and C domains of NupG, is constituted by R136, T140, F143, Q225, N228, Q261, E264, Y318, and F322. Moreover, we found that D323 is very important for substrate binding *via in vitro* uridine-binding assays using D323 mutations, although it does not have a direct contact with uridine. Our structural and biochemical data therefore provide an important framework for the mechanistic understanding of nucleoside transporters of the NHS family.**

Nucleosides play important roles in all organisms on Earth. In addition to being the basic components of nucleic acids, they are also neurotransmitters for signaling translocation (1, 2). In addition, nucleoside analogs have been suggested to be antiviral and anticancer drugs and compounds with great antibiotic activity (3).

Nucleoside homeostasis, which is mediated by nucleoside uptake and export *via* transporters, is essential for cell division and growth (4). To date, two kinds of nucleoside transporters have been found in mammals: concentrative nucleoside transporters (CNTs) and equilibrative nucleoside transporters (5). Interestingly, the nucleoside-specific outer membrane transporter Tsx and the nucleoside proton symporter (NHS) NupG are restricted in bacteria (6–8). The NHS NupG belongs to the NHS family in the major facilitate superfamily (MFS) and has been recognized as one of the prototype MFS transporters (9).

The major facilitator superfamily (MFS) is the largest protein family of transporters, which facilitate the uptake and export of various molecules across the plasma membrane (10). According to their various coupling patterns, MFS transporters can be divided into three kinds of transporters: facilitators, symporters, and antiporters (11). In recent decades, breakthroughs in structural investigations have heavily promoted the elucidation of alternating access and substrate recognition of MFS transporters; these structural studies include the series of works of the classical lactose proton symporter LacY (12–14) and investigations of glucose transporters with different conformations (15–22).

In *Escherichia coli*, nucleosides are mainly delivered *via* NupC and NupG (23). NupC, a homolog of CNTs, was found to transport pyrimidine nucleosides, adenosine, and the antibiotic showdomycin but not guanosine or inosine (24). NupG has the capacity to transport both pyrimidine and purine nucleosides efficiently but not showdomycin (24, 25). Recently, structural investigations of CNTs have helped elucidate the transport and specific nucleoside recognition mechanisms of CNTs (26–29).

Here, we report two crystal structures of the NHS transporter NupG (both at a resolution of 3.0 Å). Together with the *in vitro* binding assay, molecular docking, and molecular dynamics (MD) simulations, we identified the substrate-binding site of NupG. Moreover, we found that a negatively charged residue (D323), which indirectly coordinates with uridine, is also very important for substrate binding. This study provides an important framework for the mechanistic understanding of nucleoside recognition of NHS nucleoside transporters.

## Results

### Characterization of recombinant NupG

We overexpressed and purified recombinant NupG with monodisperse peaks in different detergent micelles (Fig. S1). To validate the function of NupG, isothermal titration calorimetry (ITC) was carried out to measure the binding between NupG and nucleosides (Fig. 1). As shown in the results, NupG

‡ These authors contributed equally to this work.
* For correspondence: Jianping Hu, hjpcdu@163.com; Bo Sun, sunb@sari.ac.cn; Dong Deng, dengd@scu.edu.cn.

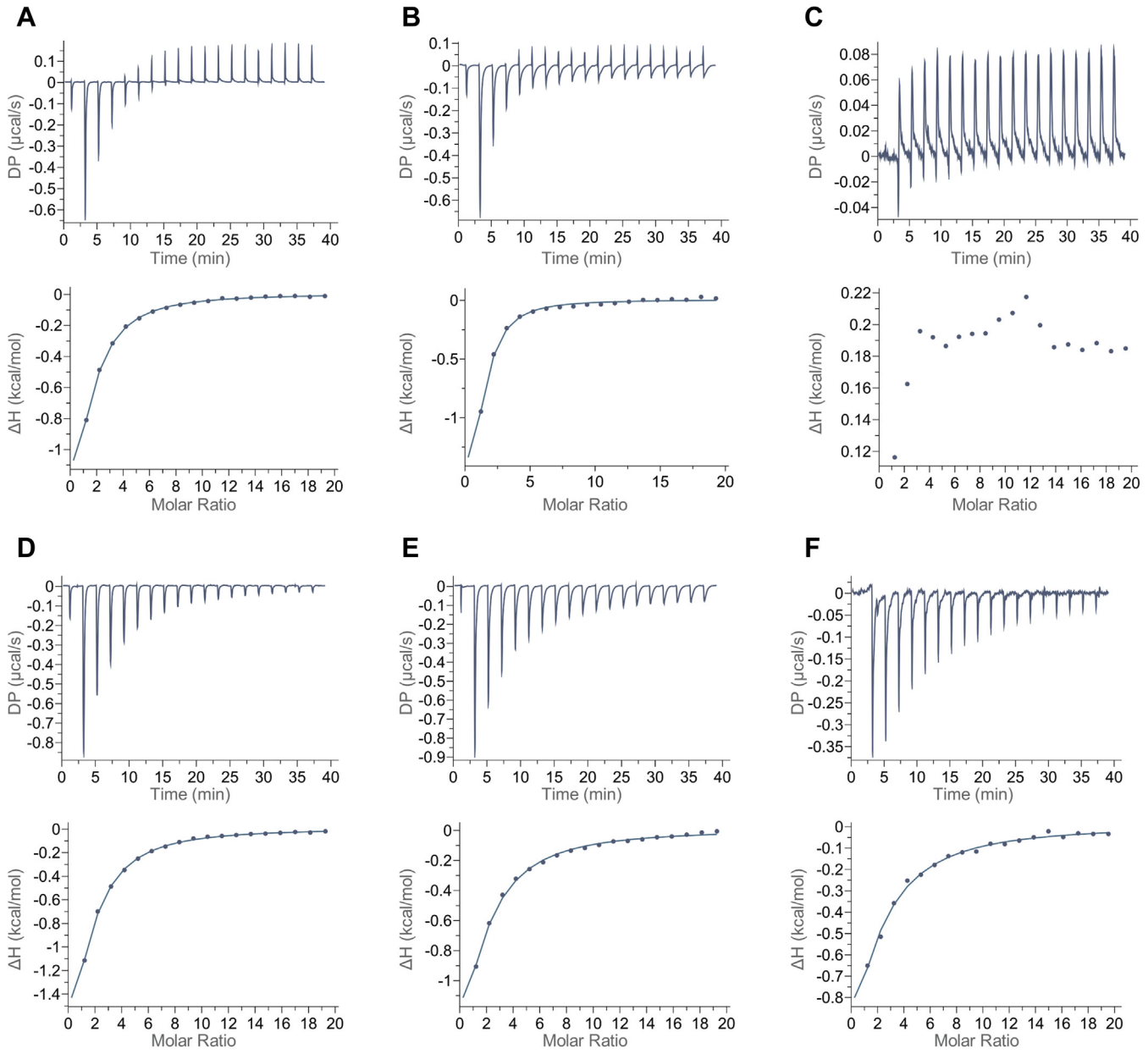


**Figure 1. Binding affinity between nucleosides and NupG measured by ITC.** *A*, binding affinity of adenosine and NupG. $K_d$ = 99.67 ± 14.57 μM. *B*, binding affinity of guanosine and NupG. $K_d$ = 46.67 ± 6.66 μM. *C*, binding affinity of xanthosine and NupG. *D*, binding affinity of cytidine and NupG. $K_d$ = 143.67 ± 19.66 μM. *E*, binding affinity of thymidine and NupG. $K_d$ = 162.5 ± 19.16 μM. *F*, binding affinity of uridine and NupG. $K_d$ = 199.67 ± 15.01 μM. ITC, isothermal titration calorimetry.

binds to adenosine with a $K_d$ of 99.67 ± 14.57 μM. NupG also binds to guanosine, thymidine, cytidine, and uridine with $K_d$ values of 46.67 ± 6.66 μM, 162.5 ± 19.16 μM, 143.67 ± 19.66 μM, and 199.67 ± 15.01 μM, respectively. Nevertheless, NupG could not bind to xanthosine (Fig. 1, Table S1), and this was also observed in a previous biochemical study (30).

We further detected the binding affinity between NupG and uridine in different buffers at various pH values. NupG binds uridine with a binding affinity of approximately 200 μM in sodium citrate at pH 5.0 and 2-(N-Morpholino) ethanesulfonic acid (MES) at pH 6.0, whereas the binding affinity dramatically reduced to approximately 3 mM in a buffer containing 25-mM Tris at pH 8.0 (Fig. S2, Table S1).

A previous study reported that NupG has the capacity to transport various nucleosides (25). Our results indicate that NupG has broad substrate selectivity and are consistent with results from a reported transport assay.

### *Overall structure of NupG*

We used X-ray crystallography to explore the substrate recognition mechanism of NupG. Extensive crystallization trials of NupG were carried out. Finally, we crystallized WT NupG and solved the structure of NupG in the apo state at a resolution of 3.0 Å (Fig. 2, Table S2). We used the molecular replacement method using the predicted structure as the search model to determine the structure of NupG (Fig. S3*C*).

Briefly, we crystallized NupG in two different space groups and collected diffraction data sets at 3.8 Å for $P2_1$ and 3.0 Å for P1. We succeeded in solving the structure of NupG with the $P2_1$ space group using molecular replacement as there was only one molecule in one asymmetric unit. In the P1 crystal, however, there are two molecules of NupG with reversed orientations in one asymmetric unit (Fig. S3*A*), and both molecules have an almost identical conformation with an RMSD of 0.21 Å over 387 Cα atoms (Fig. S3*B*). Therefore, we selected molecule A for further analyses.

Consistent with the topology prediction (25, 31), NupG has the typical MFS fold with 12 transmembrane helices (TM1-12). The N domain (TM1-6) and C domain (TM7-12) are linked by a flexible loop (Fig. 2*A*). The cavity between the N and C domains faces the cytoplasm (Fig. 2*B*). By comparing the NupG structure with well-characterized MFS transporters that have an inward-open conformation, XylE (17) and LacY (12), we found that NupG also has an inward-open conformation in the crystal structure (Fig. 2*B*).

### *Identification of potential residues involved in substrate binding*

After extensive trials, we still failed to obtain a crystal of NupG in complex with a nucleoside. Fortunately, polar substrate-binding pockets were identified in previous studies of the MFS transporters XylE and LacY (12, 13, 17). The ribose moieties of nucleosides are polar carbohydrates that are structurally similar to the natural substrates of XylE (xylose) and LacY (lactose). We speculated that all three transporters partly share a similar substrate recognition pattern. Several polar or charged residues in the cavity should directly contact the polar carbohydrate. Therefore, the polar and charged residues in the cavity may also be important for nucleoside recognition by NupG.

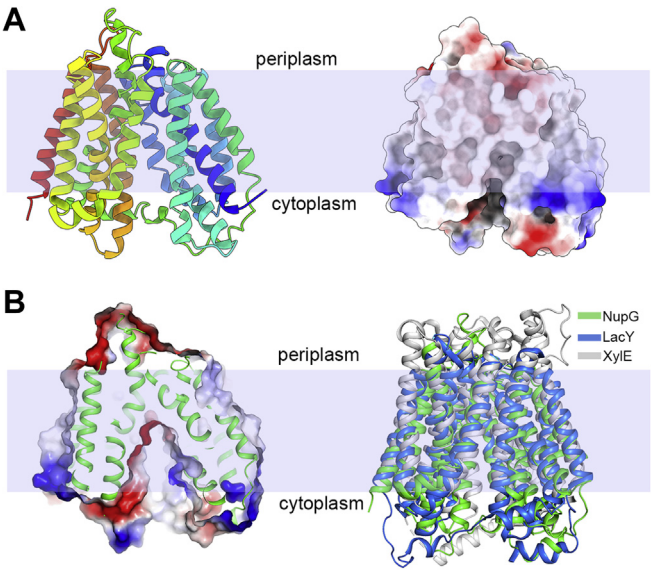


**Figure 2. Overall structure of NupG.** *A*, the ribbon representation (*left*) and surface representation (*right*) of NupG. *B*, superposition of LacY (*blue*), XylE (*gray*), and NupG (*green*).

To identify the residues involved in substrate binding, we first investigated several polar residues (Q225, N228, E264, and D323) in the cavity of NupG (Fig. 3*A*). Mutants were generated, and the uridine binding of these constructs was detected *via* ITC. As shown in the results, Q225A had a similar binding affinity for uridine ($K_d$ at 227.67 ± 88.34 μM) as WT NupG, whereas N228A and E264A dramatically reduced the uridine-binding ability, suggesting that N228 and E264 are essential for nucleoside binding. Surprisingly, $NupG_{D323A}$ bound to uridine with a $K_d$ of 9.67 ± 2.87 μM, which is a 20-fold increase in the binding affinity compared with that of $NupG_{WT}$ (Fig. 3*B*, Table S1). Considering the increased uridine-binding capacity of $NupG_{D323A}$, we crystallized $NupG_{D323A}$ under nucleoside-containing conditions and solved the structure of $NupG_{D323A}$ at a resolution of 3.0 Å (Table S2). The superposition of the $NupG_{D323A}$ and $NupG_{WT}$ structures showed that they had identical conformations, with an RMSD of 0.3 Å over 384 Cα atoms (Fig. S3*D*). Unfortunately, no visible electron density of uridine was observed in the central cavity (Fig. S3*E*).

### *Putative substrate-binding site*

We continued to explore the nucleoside-binding site of NupG *via* molecular docking (Fig. 4). Considering the higher binding affinity between $NupG_{D323A}$ and uridine, we first generated a uridine docking model based on the $NupG_{D323A}$ structure using Discovery Studio 3.5 software (Fig. 4*A*). Then, we confirmed the stability of the system by analyzing a series of conventional structural convergence parameters based on the MD simulation trajectory (Fig. 4*B*). As shown in Figure 4*B*, the potential energy reaches equilibrium soon after removing the constraints, and its mean value and SD are $-8.93 \times 10^5$ and $0.07 \times 10^5$ kcal $mol^{-1}$, respectively; the uridine-bound system tends to be stable after 10 ns with an RMSD of 0.19 ± 0.08 nm; according to the change in the gyration radius over the simulation time, the system tends to equilibrate after 30 ns, with a small fluctuation in the amplitude (approximately 0.01 nm), which indicates that the system experienced a slight expansion and contraction during this period; regarding the distribution of the RMSF on different amino acid residue $C_\alpha$ atoms, the overall RMSF value is low and the atomic motion range is not large. All the above simulation results suggest that uridine-bound NupG is relatively stable.

In the uridine-bound model, the uridine molecule was docked into the central cavity, which has direct contact with the side chains of residues from the N and C domains (Fig. 4*A*). Nucleosides are comprised of two basic components, namely, the ribose and base. In the docking model, R136 and T140 from the N domain and E264 from the C domain form hydrogen bonds with the ribose moiety of uridine. Interestingly, these three residues are identical in three members of the NHS family (NupG, XapB, and YegT). These three transporters have different nucleoside selectivity, but this is understandable for the recognition of invariable ribose by identical residues in the cavity of NHS transporters. The further ConSurf evolutionary analysis using 150 homologs of NupG also reveals that R136, T140, and E264 are highly

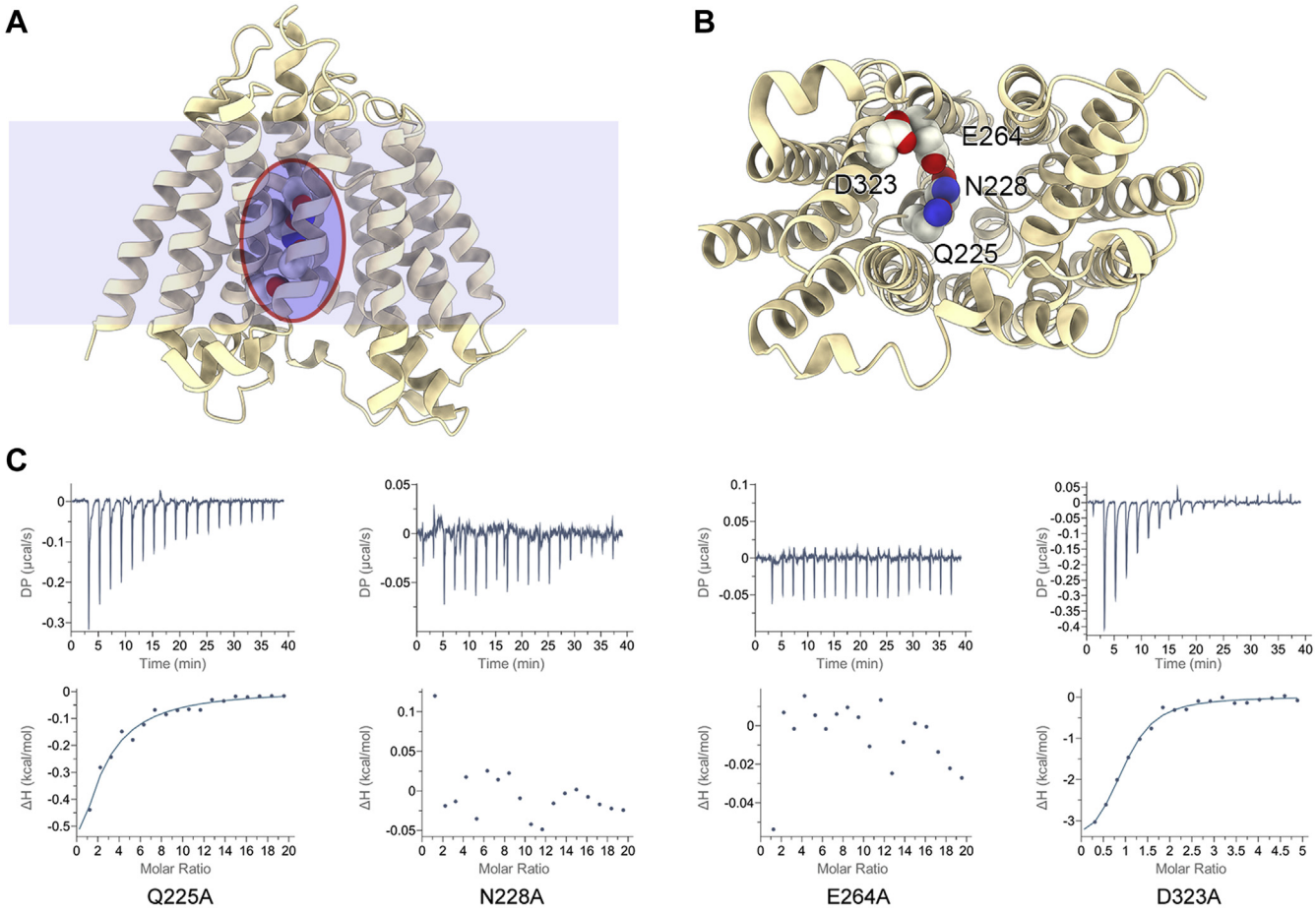


**Figure 3. Identification of potential residues involving in substrates binding.** *A*, the side view of NupG. The overall structure is represented as *ribbons*, and potential residues involved in substrates binding are represented as *spheres*. *B*, the cytoplasmic view of NupG. The overall structure is represented by *ribbons*, and potential residues involved in substrates binding are represented as *spheres*. *C*, uridine binding affinity of NupG variants measured by ITC. $K_d$ = 227.67 ± 88.34 μM for Q225A. $K_d$ = 9.67 ± 2.87 μM for D323A. ITC, isothermal titration calorimetry.

conserved (Fig. S6). Furthermore, Q225, N228, Q261, and Y318 from the C domain form hydrogen bonds with the base of uridine. Unlike the contact with ribose, the residues involving base recognition are relatively variable. With the exception of Q261, the Q225, N228, and Y318 residues of NupG are A226, Y310, and H315 in YegT (Fig. S5).The conservation scores of Q225 and N228 are 6 and 7, respectively, as shown by the ConSurf evolutionary analysis (Fig. S6). This observation indicates that these residues determine the specifications of nucleoside recognition. In addition, there are two conserved aromatic residues around uridine (Fig. 4*A*, Fig. S6).

To further verify the docking results, *in vitro* binding assays were carried out. We constructed a series of single point mutations of NupG: R136A, T140A, F143A, Q225A, N228A, Q261A, E264A, Y318A, and F322A. As the ITC results showed, all mutant versions of NupG, except $NupG_{Q225A}$, abolished the binding affinity between NupG and uridine (Fig. 5, Table S1). This result indicated that the hydrogen-bound interactions between these residues and uridine are essential for substrate recognition. Interestingly, F143A and F322A also eliminated the binding affinity between NupG and uridine, indicating that F143 and F322 are also essential for substrate binding. The surrounding aromatic residues involved in substrate recognition of nucleoside transporters, such as F366 of vcCNT (27) and F564 of hCNT3 (29), are a common feature. F143 and F322 might form π–π interactions with uridine and restrict the specific orientation of the nucleosides.

## Discussion

In a previous study, N114 was predicted to be important in the recognition of nucleoside transport by NupG (31, 32). However, in our study, N114 is far away from uridine. In addition, N114A also did not influence the binding affinity between NupG and uridine (Fig. S4*B*). In the structure of NupG, N114 is in TM4 and corresponds to E126 in LacY, which is indispensable for substrate binding and might form a charge pair with R144 of LacY (12, 33).

Interestingly, there are three NHS transporters, NupG (8), XapB (34), and YegT (9), that are found in *E. coli*. XapB shares 58% sequence identity and 76% sequence similarity with NupG (Fig. S5) and was identified as a xanthosine-specific transporter (30); however, the natural substrate of YegT should be further investigated, although YegT shares 27% sequence identity and 50% sequence similarity with NupG (Fig. S5). The residues

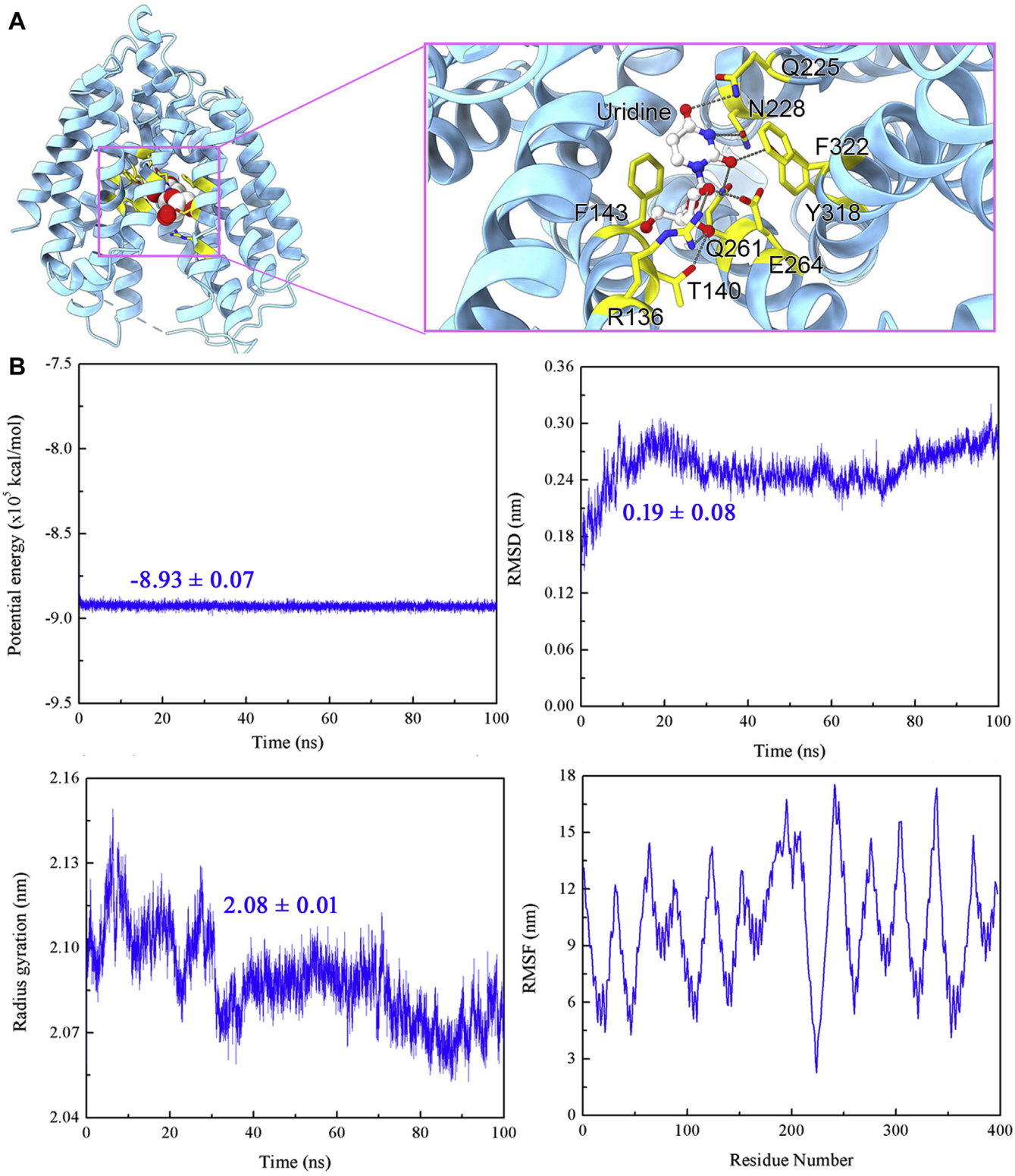


**Figure 4. Putative substrate-binding site of NupG.** *A*, the docking model of the $NupG_{D323A}$–uridine complex. *Left*, the overall structure is represented as *ribbons*, and uridine is represented as *spheres*. *Right*, detailed interaction between putative substrate binding sites (*yellow sticks*) and uridine (*white stick*). *B*, MD simulations of the docking model. MD, molecular dynamics.

involved in the uridine binding pocket of NupG are identical to those of XapB. A previous biochemical study suggested that the preferred substrate of XapB is xanthosine, whereas NupG could not bind or transport xanthosine (Fig. 1). Therefore, other residues surrounding the pocket also contribute to substrate recognition.

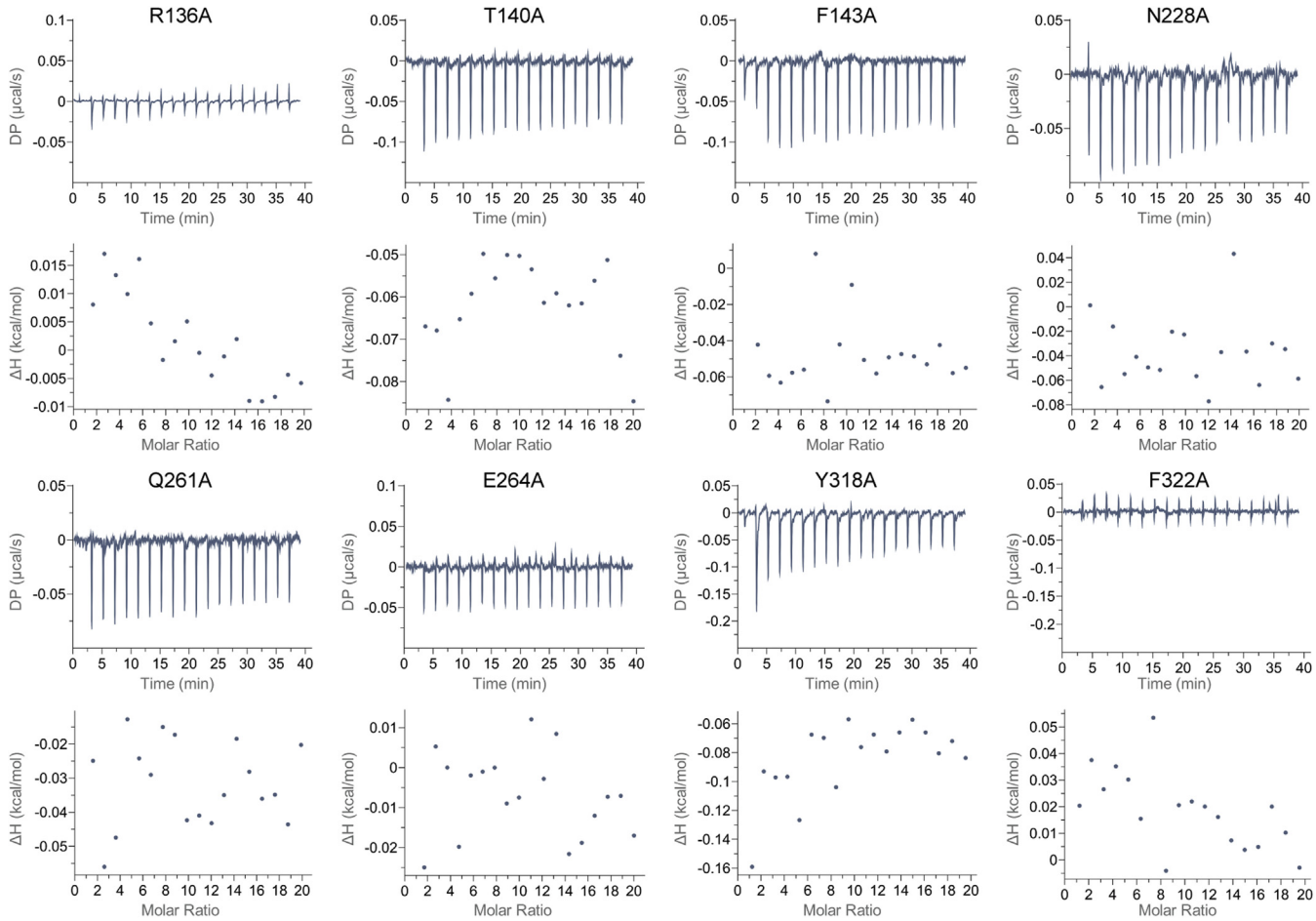


**Figure 5. Uridine binding affinity of NupG variants measured by ITC.** Details can be found in Experimental procedures. Each mutation of NupG is labeled above the corresponding experimental result. ITC, isothermal titration calorimetry.

During this study, we found that the D323A mutant enhances the binding affinity between NupG and uridine (Fig. 2*B*). This result indicated that D323 is an important residue for nucleoside transport, although D323 does not directly contact the substrate-binding site. Further investigations showed that the D323A mutant maintained a similar uridine-binding affinity in different buffers with various pH values, while $NupG_{WT}$ decreased its binding affinity at a basic pH (Fig. S2) (Fig. S4). This property is similar to that of the mutated lactose proton symporter LacY E325A (35, 36). In the case of LacY, E325 and K319 were identified as protonation sites, and the uncharged side chains of E325 and K319 retain a high affinity with lactose, even at an alkaline pH (35, 36). Therefore, we speculated that D323 may be the proton-escaping site of NupG during the proton-coupling procedure. Interestingly, $NupG_{D323N}$, which mimics the protonation state at position 323, bound to uridine with a reducing $K_d$ of 1109 ± 192.21 μM (Fig. S4*B*, Table S1). Therefore, more structural and biochemical investigations should be carried out to elucidate how D323 couples substrate binding and protonation.

In this study, we solved the first structure of an NHS transporter NupG. Together with the MD simulations and biochemical assays, we identified the nucleoside binding site of NupG. Our study provides a framework for understanding the transport and substrate recognition mechanisms of NHS transporters.

## Experimental procedures

### *Protein purification*

Full-length nupG was cloned from *E. coli* K12 and subcloned into pET21b. Overexpression of NupG was induced in *E. coli* C43(DE3) cells by 0.2-mM IPTG when the cell density reached an absorbance at 600 nm of 1.0. After incubation for 15 h at 18 °C, the cells were harvested and homogenized in the buffer containing 25-mM MES (pH 6.0) and 150- mM NaCl. The membranes were collected and incubated for 2 h with 2% (w/v) dodecyl-β-D-maltopyranoside (DDM, Anatrace) at 4 °C. After centrifugation at 17,000 rpm for 30 min, the supernatant was collected and loaded onto Ni-NTA affinity resin (Qiagen) and rinsed with the buffer containing 25-mM MES (pH 6.0), 150-mM NaCl, 20-mM imidazole, and 0.02% DDM. The protein was eluted with a buffer containing 25-mM MES (pH 6.0), 150-mM NaCl, 250-mM imidazole and 0.4% NG. The protein was concentrated to approximately 20 mg/ml before further purification by gel filtration (Superdex200 10/300 increase column; GE Healthcare) in the buffer containing

25-mM MES (pH 6.0), 150-mM NaCl, and 0.4% NG. The peak fractions were collected and concentrated to approximately 30 mg/ml for further crystallization. For the binding assay, NupG was purified in the buffer containing 0.02% DDM in all steps. All mutations were generated by standard two-step PCR and purified using the same protocol.

### Crystallization

Both WT and D323A NupG were crystallized by the mesophase method (37, 38). A total of 30 mg/ml protein was mixed with monoolein (M-239, Nu-Chek) at a 1:1.5 protein to lipid ratio (w/w) using a syringe lipid mixer. Briefly, the 60 nl of the meso phase was covered with 600 nl of crystallization buffer for each condition and sealed in glass sandwich plates (Shanghai FAstal BioTech). Crystals grew at 1 week in 0.1 M sodium citrate (pH 5.0) and 28% PEG300 for WT NupG $P2_1$ structure, in 0.1 M NaCl, 0.1 M MgCl2, 0.1 M sodium citrate (pH 5.0), and 30% PEG600 for WT NupG P1 structure, and in 0.1 M NaCl, 0.1 M $MgCl_2$, 0.1 M MES (pH 6.0), and 30% PEG550 MME for $NupG_{D323A}$. Crystals were harvested and frozen in liquid nitrogen.

### Structure determination

The diffraction data were collected at the beamline BL18U1 of SSRF and processed with XDS (39). The data were scaled by using Aimless in the CCP4 program suite (40). The WT NupG structure was solved by molecular replacement using the predicted structure of NupG as the search model. First, the predicted structure of NupG was generated using the Robetta server (http://robetta.bakerlab.org) (41). The primary predicted model was further modified as polyalanine and divided into the N domain (TM1-6) and C domain (TM7-12) before molecular replacement by phenix.phaser (42, 43). A good initial solution was obtained by using the P121 crystal form data (diffracting to 3.8 Å) (Table S1) with one molecule in the asymmetric unit. After multiple rounds of manual building and refining, the initial model was good enough to generate a molecular replacement solution for data of the P1 crystal form (3 Å) with two NupG molecules in the asymmetric unit. The complete structure of NupG was obtained by using iterative manual building in coot (44) and refinement in phenix.refine (Table S2).

### ITC

The nucleoside binding of NupG was measured with a MicroCal iTC200 at 25 °C. The purified NupG proteins were concentrated to 40 to 60 μM for ITC. The titration data were analyzed using the one-site binding model, and the first injection was removed. The titration of nucleosides into the buffer was deducted. All the experiments were repeated three times. A representative result was selected to present, and the means ± SD of $K_d$ are calculated and summarized in Table S1.

### Molecular docking

In general, molecular docking has been widely used to describe the "best-fit" orientation of a ligand binding to a particular protein and to predict the complex structure (45). Here, the uridine molecule was constructed with the ChemBio3D Ultra 12.0 package, and then its energy was minimized under the MM2 force field with an RMS less than 0.0001 kcal $mol^{-1}$ $Å^{-1}$. After the optimization of the molecular mechanics, Gaussian 09 (46) was adopted to refine the structure again at a higher level of quantum mechanics. Energy optimization and molecular docking of the target protein (*i.e.*, $NupG_{D323A}$) were carried out with the Prepare Protein and CDOCKER modules in Discovery Studio 3.5 software, respectively. In addition, the docking center (x: −18.314, y: −15.508, z: 5.605) and search radius (1.2 nm) were both preset.

### MD simulation

MD simulation at 300 K was performed for $NupG_{D323A}$ with AMBER 18 software (47) and the ff16SB force field (48). A total of 9599 water molecules and one sodium molecule were added to the system using the TIP3P water model (49) with a box boundary of 8.0 Å. Before the MD simulation, the following two-stage energy optimization method was carried out for $NupG_{D323A}$: (1) the solute was constrained with a force constant of 500 kcal $mol^{-1}$ $Å^{-2}$ containing 3000 steps in the steepest descent and 5000 steps in the conjugate gradient minimization; (2) after removing the geometry constraints, the second optimization was also composed of 3000 steps in the steepest descent and 5000 steps in the conjugate gradient minimization.

After energy minimization, the MD simulation was started and was divided into the following two procedures: (1) a 5-ns constrained MD was performed with a constraint force constant of 10 kcal $mol^{-1}$ $Å^{-2}$, and the temperature gradually increased from 0 to 300 K; (2) a 50-ns unconstrained productive MD simulation was performed, adopting the SHAKE algorithm (50) to constrain the hydrogen atoms. In addition, the nonbonded interaction radius was set as 8 Å, the integration step was set to 2 fs, and the conformational snapshot was collected every 10 ps. Thus, a total of 5500 conformations were selected for the following structural analyses.

## Data availability

The atomic coordinates have been deposited in the Protein Data Bank (PDB accession code: 7DL9 for $NupG_{WT}$ and 7DLA for $NupG_{D323A}$). All other data are contained within the article.

*Supporting information*—This article contains supporting information.

*Acknowledgments*—We thank the staff at Shanghai Synchrotron Radiation Facility (SSRF) beamline BL18U1. This work was supported by fund from the National Natural Science Foundation of China (31971132).

*Author contributions*—D. D. conceived the project. J. H., B. S., and D. D. designed all of the experiments. C. W., J. L., and J. Z. expressed, purified, and crystallized NupG. Q. X., Q.W., and B. S.

collected and processed the data and solved the structure. H. D. and J. H. performed molecular docking and MD simulation. L. G., J. H., B. S., and D. D. wrote the manuscript. All authors discussed the results and commented on the manuscript.

*Conflict of interest*—The authors declare that no competing interests exist.

*Abbreviations*—The abbreviations used are: CNT, concentrative nucleoside transporter; DDM, dodecyl-β-D-maltopyranoside; ITC, isothermal titration calorimetry; MES, 2-(N-Morpholino) ethanesulfonic acid.

## References


1. Parkinson, F. E., Damaraju, V. L., Graham, K., Yao, S. Y., Baldwin, S. A., Cass, C. E., and Young, J. D. (2011) Molecular biology of nucleoside transporters and their distributions and functions in the brain. *Curr. Top. Med. Chem.* **11**, 948–972
2. Fredholm, B. B., Chen, J. F., Cunha, R. A., Svenningsson, P., and Vaugeois, J. M. (2005) Adenosine and brain function. *Int. Rev. Neurobiol.* **63**, 191–270
3. Serpi, M., Ferrari, V., and Pertusati, F. (2016) Nucleoside derived antibiotics to fight microbial drug resistance: New utilities for an established class of drugs? *J. Med. Chem.* **59**, 10343–10382
4. Molina-Arcas, M., Casado, F. J., and Pastor-Anglada, M. (2009) Nucleoside transporter proteins. *Curr. Vasc. Pharmacol.* **7**, 426–434
5. Young, J. D., Yao, S. Y., Baldwin, J. M., Cass, C. E., and Baldwin, S. A. (2013) The human concentrative and equilibrative nucleoside transporter families, SLC28 and SLC29. *Mol. Aspects Med.* **34**, 529–547
6. Nieweg, A., and Bremer, E. (1997) The nucleoside-specific Tsx channel from the outer membrane of Salmonella typhimurium, Klebsiella pneumoniae and Enterobacter aerogenes: Functional characterization and DNA sequence analysis of the tsx genes. *Microbiology (Reading)* **143**(Pt 2), 603–615
7. Ye, J., and van den Berg, B. (2004) Crystal structure of the bacterial nucleoside transporter Tsx. *EMBO J.* **23**, 3187–3195
8. Westh Hansen, S. E., Jensen, N., and Munch-Petersen, A. (1987) Studies on the sequence and structure of the Escherichia coli K-12 nupG gene, encoding a nucleoside-transport system. *Eur. J. Biochem.* **168**, 385–391
9. Cabrita, M. A., Baldwin, S. A., Young, J. D., and Cass, C. E. (2002) Molecular biology and regulation of nucleoside and nucleobase transporter proteins in eukaryotes and prokaryotes. *Biochem. Cell Biol.* **80**, 623–638
10. Quistgaard, E. M., Low, C., Guettou, F., and Nordlund, P. (2016) Understanding transport by the major facilitator superfamily (MFS): Structures pave the way. *Nat. Rev. Mol. Cell Biol.* **17**, 123–132
11. Yan, N. (2015) Structural biology of the major facilitator superfamily transporters. *Annu. Rev. Biophys.* **44**, 257–283
12. Abramson, J., Smirnova, I., Kasho, V., Verner, G., Kaback, H. R., and Iwata, S. (2003) Structure and mechanism of the lactose permease of Escherichia coli. *Science* **301**, 610–615
13. Kumar, H., Kasho, V., Smirnova, I., Finer-Moore, J. S., Kaback, H. R., and Stroud, R. M. (2014) Structure of sugar-bound LacY. *Proc. Natl. Acad. Sci. U. S. A.* **111**, 1784–1788
14. Madej, M. G., and Kaback, H. R. (2014) The life and times of Lac permease: crystals ain't everything, but they certainly do help. In: Krämer, R., Ziegler, C., eds. *Membrane Transport Mechanism: 3D Structure and Beyond*, Springer Berlin Heidelberg, Berlin, Heidelberg: 121–158
15. Deng, D., Xu, C., Sun, P., Wu, J., Yan, C., Hu, M., and Yan, N. (2014) Crystal structure of the human glucose transporter GLUT1. *Nature* **510**, 121–125
16. Deng, D., Sun, P., Yan, C., Ke, M., Jiang, X., Xiong, L., Ren, W., Hirata, K., Yamamoto, M., Fan, S., and Yan, N. (2015) Molecular basis of ligand recognition and transport by glucose transporters. *Nature* **526**, 391–396
17. Sun, L., Zeng, X., Yan, C., Sun, X., Gong, X., Rao, Y., and Yan, N. (2012) Crystal structure of a bacterial homologue of glucose transporters GLUT1-4. *Nature* **490**, 361–366
18. Wisedchaisri, G., Park, M.-S., Iadanza, M. G., Zheng, H., and Gonen, T. (2014) Proton-coupled sugar transport in the prototypical major facilitator superfamily protein XylE. *Nat. Commun.* **5**, 4521
19. Quistgaard, E. M., Löw, C., Moberg, P., Trésaugues, L., and Nordlund, P. (2013) Structural basis for substrate transport in the GLUT-homology family of monosaccharide transporters. *Nat. Struct. Mol. Biol.* **20**, 766–768
20. Qureshi, A. A., Suades, A., Matsuoka, R., Brock, J., McComas, S. E., Nji, E., Orellana, L., Claesson, M., Delemotte, L., and Drew, D. (2020) The molecular basis for sugar import in malaria parasites. *Nature* **578**, 321–325
21. Madej, M. G., Sun, L., Yan, N., and Kaback, H. R. (2014) Functional architecture of MFS D-glucose transporters. *Proc. Natl. Acad. Sci. U. S. A.* **111**, E719–E727
22. Jiang, X., Yuan, Y., Huang, J., Zhang, S., Luo, S., Wang, N., Pu, D., Zhao, N., Tang, Q., Hirata, K., Yang, X., Jiao, Y., Sakata-Kato, T., Wu, J. W., Yan, C., *et al.* (2020) Structural basis for blocking sugar uptake into the malaria parasite Plasmodium falciparum. *Cell* **183**, 258–268.e212
23. Munch-Petersen, A., Mygind, B., Nicolaisen, A., and Pihl, N. J. (1979) Nucleoside transport in cells and membrane vesicles from Escherichia coli K12. *J. Biol. Chem.* **254**, 3730–3737
24. Munch-Petersen, A., and Mygind, B. (1976) Nucleoside transport systems in Escherichia coli K12: Specificity and regulation. *J. Cell Physiol.* **89**, 551–559
25. Xie, H., Patching, S. G., Gallagher, M. P., Litherland, G. J., Brough, A. R., Venter, H., Yao, S. Y., Ng, A. M., Young, J. D., Herbert, R. B., Henderson, P. J., and Baldwin, S. A. (2004) Purification and properties of the Escherichia coli nucleoside transporter NupG, a paradigm for a major facilitator transporter sub-family. *Mol. Membr. Biol.* **21**, 323–336
26. Johnson, Z. L., Cheong, C. G., and Lee, S. Y. (2012) Crystal structure of a concentrative nucleoside transporter from Vibrio cholerae at 2.4 A. *Nature* **483**, 489–493
27. Johnson, Z. L., Lee, J. H., Lee, K., Lee, M., Kwon, D. Y., Hong, J., and Lee, S. Y. (2014) Structural basis of nucleoside and nucleoside drug selectivity by concentrative nucleoside transporters. *Elife* **3**, e03604
28. Hirschi, M., Johnson, Z. L., and Lee, S.-Y. (2017) Visualizing multistep elevator-like transitions of a nucleoside transporter. *Nature* **545**, 66–70
29. Zhou, Y., Liao, L., Wang, C., Li, J., Chi, P., Xiao, Q., Liu, Q., Guo, L., Sun, L., and Deng, D. (2020) Cryo-EM structure of the human concentrative nucleoside transporter CNT3. *PLoS Biol.* **18**, e3000790
30. Norholm, M. H., and Dandanell, G. (2001) Specificity and topology of the Escherichia coli xanthosine permease, a representative of the NHS subfamily of the major facilitator superfamily. *J. Bacteriol.* **183**, 4900–4904
31. Patching, S. G., Baldwin, S. A., Baldwin, A. D., Young, J. D., Gallagher, M. P., Henderson, P. J., and Herbert, R. B. (2005) The nucleoside transport proteins, NupC and NupG, from Escherichia coli: Specific structural motifs necessary for the binding of ligands. *Org. Biomol. Chem.* **3**, 462–470
32. Vaziri, H., Baldwin, S. A., Baldwin, J. M., Adams, D. G., Young, J. D., and Postis, V. L. (2013) Use of molecular modelling to probe the mechanism of the nucleoside transporter NupG. *Mol. Membr. Biol.* **30**, 114–128
33. Sahin-Tóth, M., le Coutre, J., Kharabi, D., le Maire, G., Lee, J. C., and Kaback, H. R. (1999) Characterization of Glu126 and Arg144, two residues that are indispensable for substrate binding in the lactose permease of Escherichia coli. *Biochemistry* **38**, 813–819
34. Seeger, C., Poulsen, C., and Dandanell, G. (1995) Identification and characterization of genes (xapA, xapB, and xapR) involved in xanthosine catabolism in Escherichia coli. *J. Bacteriol.* **177**, 5506–5516
35. Smirnova, I., Kasho, V., Sugihara, J., Choe, J. Y., and Kaback, H. R. (2009) Residues in the H+ translocation site define the pKa for sugar binding to LacY. *Biochemistry* **48**, 8852–8860
36. Grytsyk, N., Sugihara, J., Kaback, H. R., and Hellwig, P. (2017) pKa of Glu325 in LacY. *Proc. Natl. Acad. Sci. U. S. A.* **114**, 1530–1535
37. Caffrey, M., and Cherezov, V. (2009) Crystallizing membrane proteins using lipidic mesophases. *Nat. Protoc.* **4**, 706–731

38. Ma, P., Weichert, D., Aleksandrov, L. A., Jensen, T. J., Riordan, J. R., Liu, X., Kobilka, B. K., and Caffrey, M. (2017) The cubicon method for concentrating membrane proteins in the cubic mesophase. *Nat. Protoc.* **12**, 1745–1762
39. Kabsch, W. (2010) XDS. *Acta Crystallogr. D Biol. Crystallogr.* **66**, 125–132
40. Winn, M. D., Ballard, C. C., Cowtan, K. D., Dodson, E. J., Emsley, P., Evans, P. R., Keegan, R. M., Krissinel, E. B., Leslie, A. G., McCoy, A., McNicholas, S. J., Murshudov, G. N., Pannu, N. S., Potterton, E. A., Powell, H. R., *et al.* (2011) Overview of the CCP4 suite and current developments. *Acta Crystallogr. D Biol. Crystallogr.* **67**, 235–242
41. Kim, D. E., Chivian, D., and Baker, D. (2004) Protein structure prediction and analysis using the Robetta server. *Nucleic Acids Res.* **32**, W526–531
42. McCoy, A. J., Grosse-Kunstleve, R. W., Adams, P. D., Winn, M. D., Storoni, L. C., and Read, R. J. (2007) Phaser crystallographic software. *J. Appl. Crystallogr.* **40**, 658–674
43. Adams, P. D., Afonine, P. V., Bunkoczi, G., Chen, V. B., Davis, I. W., Echols, N., Headd, J. J., Hung, L. W., Kapral, G. J., Grosse-Kunstleve, R. W., McCoy, A. J., Moriarty, N. W., Oeffner, R., Read, R. J., Richardson, D. C., *et al.* (2010) Phenix: A comprehensive Python-based system for macromolecular structure solution. *Acta Crystallogr. D Biol. Crystallogr.* **66**, 213–221
44. Emsley, P., and Cowtan, K. (2004) Coot: Model-building tools for molecular graphics. *Acta Crystallogr. D Biol. Crystallogr.* **60**, 2126–2132
45. Ahmed, H., Ihmaid, S., Omar, A., Shehata, M., Rateb, H., Zayed, M., Ahmed, S., and Elaasser, M. (2018) Design, synthesis, molecular docking of new lipophilic acetamide derivatives affording potential anticancer and antimicrobial agents. *Bioorg. Chem.* **76**, 332–342
46. Frisch, M. J., Trucks, G. W., Schlegel, H. B., Scuseria, G. E., Robb, M. A., Cheeseman, J. R., Scalmani, G., Barone, V., Mennucci, B., Petersson, G. A., Nakatsuji, H., Caricato, M., Li, X., Hratchian, H. P., Izmaylov, A. F., *et al.* (2009) *"Gaussian 09," Revision A.1*, Gaussian, Inc., Wallingford
47. Case, I. Y. B.-S. D. A., Brozell, S. R., Cerutti, D. S., Cheatham, T. E., III, Cruzeiro, V. W. D., Darden, T. A., Duke, R. E., Ghoreishi, D., Gilson, M. K., Gohlke, H., Goetz, A. W., Greene, D., Harris, R., Homeyer, N., Izadi, S., *et al.* (2018) *Amber*, University of California, San Francisco
48. Maier, J. A., Martinez, C., Kasavajhala, K., Wickstrom, L., Hauser, K. E., and Simmerling, C. (2015) ff14SB: Improving the accuracy of protein side chain and backbone parameters from ff99SB. *J. Chem. Theor. Comput.* **11**, 3696–3713
49. Jorgensen, W. L., Chandrasekhar, J., Madura, J. D., Impey, R. W., and Klein, M. L. (1983) Comparison of simple potential functions for simulating liquid water. *J. Chem. Phys.* **79**, 926–935
50. Ryckaert, J.-P., Ciccotti, G., and Berendsen, H. J. C. (1977) Numerical integration of the cartesian equations of motion of a system with constraints: Molecular dynamics of n-alkanes. *J. Comput. Phys.* **23**, 327–341